Designing and analyzing two non-invasive current sensors using Ampere Force Law (AFL)

Mohammad Reza Zamani Kouhpanji*

Electrical and Computer Engineering Department, University of Minnesota Twin Cities, Minneapolis, MN 55455, USA.

Abstract

Here two different non-invasive current sensors are proposed, modeled and analyzed. The current sensors are based on the Ampere Force Law (AFL), defining the magnetic force between two parallel wire carrying currents. These current sensors can be used for detecting/sensing DC and AC currents as well as their combination in a single wire or multiple wires, and they do not rely on any permanent magnets for operation. In the first configuration, there are two microbeams, in which one of them is at the vicinity of the wire and undergoes the mechanical vibrations due to the magnetic force between the wire and the microbeam. The movement of the microbeam while it is generating a magnetic field induces a current inside another microbeam, which is stationary, as the output signal of the current sensor. In the second configuration, a single composite piezoelectric microbeam is used. The magnetic force between the wire and the piezoelectric microbeam leads the piezoelectric microbeam to move, thus it produces a voltage. Both configurations present extremely low power consumption, which is not dependent on the sensitivity of the current sensors. The dynamic response, sensitivity and power consumption of the current sensors are investigated, compared and discussed.

Keywords: non-invasive current sensors; extremely low power consumption; high sensitivity; dynamic response.

1 Introduction

Nowadays the uncountable benefits of quantum effects and size-dependency phenomena have become a great motivation for scientists to miniaturize the electronic and photonic devices. This trend made the nanotechnologies to become the most dominant research field in all over the world. However, these miniaturized electronic and photonic nanodevices require highly accurate nano/microelectromechanical devices (NEMS/MEMS), such as current sensors, to precisely control their power in order to reach their maximum quantum efficiency (Cao, Jian Tian, & Wang, 2017; Kouhpanji, Behzadirad, Feezell, & Busani, 2018; Reza & Kouhpanji, 2017; W Xian et al., 2017; Zamani Kouhpanji, Behzadirad, & Busani, 2017; Zamani Kouhpanji & Jafaraghaei, 2017). Moreover, it should be emphasized that the applications of the current sensors are not limited only to the nanotechnologies. They are also a fundamental part of power networks, where any over/under flowing current damages the whole network (Sensitivity, 2014).

A vast number of studies on the current sensors was mainly manifested by early studies of Edwin Hall in 1879 (Sherman, Wright, & White, 2016), followed by several intellectual non-invasive current sensors, such as magnetoresistive sensor (Leland, White, & Wright, 2008), Rogowski coil sensors (Chattock, 1887; Ward & Exon, 1993), and Hall effect sensors (Ramsden, 2011; Ziegler, Woodward, Iu, & Borle, 2009). The state-of-art of the non-

* Corresponding author, Email: zaman022@umn.edu, Tel.: +1(618)-305-9636.

invasive current sensors is that they can measure the current flowing inside a wire without the need of being inserted in the circuit as it used to be the case for the traditional current sensors.

This advantageous of the non-invasive current sensors makes them an excellent candidate for health monitoring and diagnostics of electrical circuits, from industrial and household scales to portable electronic devices such as cellphones. For diagnostic purposes of industrial equipment, the current sensor can be easily placed next to wires to measure the flowing current without the need of cutting the wire. This feature reduces diagnostic time and facilitates the process. For household applications, the current sensor can be used to monitor the electrical consumption for controlling power consumption at peak times. Or, if there is an electrical discharge, the current flow suddenly changes, thus the current sensor can shut off the equipment for safety purposes. For portable electronic devices, these types of current sensors can monitor power consumption with different applications. In the case when the device is running out of battery, the current sensor can show notifications to the user to close the application for saving battery. In addition to the high-power consumption of the traditional current sensors, they need to encircle wires to sense the current. This practical limitation causes these current sensors not to be used when there is more than one current in the nanodevice or network. Attempts to improve the performance of the current sensor resulted in developments of a new designs of the current sensors such as magnetic tunnel junction (Breth et al., 2011; Julliere, 1975), piezoresistive sensors (Lin & Du, 2011), and delta-f resonant sensors (Hui, Nan, Sun, & Rinaldi, 2013; Wang & Maeda, 2015). In a more realistic evaluation of these current sensors; however, they represented very small power consumption in some cases, there is always a tradeoff between the power consumption, the sensor's sensitivity, and the magnetic field saturation of these current sensors (Sherman et al., 2016).

To avoid the tradeoff, a new family of the current sensors emerged that they do not require any power supply (Leland, White, & Wright, 2006; Leland et al., 2008; Wang et al., 2017). This family of the current sensors consists of a permanent magnet and a piezoelectric microbeam, where the permanent magnet is fixed on the tip of the piezoelectric microbeam. In these current sensors, the interaction between the permanent magnet and the magnetic field of the wire results in a mechanical force applying on the piezoelectric microbeam. The main drawback of these current sensors is the durability and reliability of the sensors. That is why the characterization and performance of the sensors highly depend on the magnetic properties of the permanent magnet (Shang et al., 2017) and the piezoelectric properties of the microbeam that degenerate over time (Jackson, Olszewski, O'Murchu, & Mathewson, 2017; Olszewski, Houlihan, Blake, Mathewson, & Jackson, 2017; Zamani Kouhpanji, 2018a). Furthermore, this type of current sensors is mainly usable for paired-wires configurations, where there is a uniform magnetic field gradient. For the case of a single wire, not only the magnetic field gradient is nonuniform but it also is nonlinear in the space surrounding the wires, where the position and orientation of the current sensor must be precisely determined (Leland et al., 2008; Weikang Xian & Wang, 2017) in order to have a decent accuracy and sensitivity.

Consequently, the first motivation of this work is to design and analyze two alternative non-invasive current sensors without any limitations on the number of wires carrying unknown currents. The second motivation is to enhance the performance and reliability of the current sensors by avoiding the uncertainties due to the properties of the materials used in the current sensor. To do so, two different current sensor configurations are proposed, designed and analyzed. In both configurations, instead of using a permanent magnet, a microbeam carrying a current was used to interact with the magnetic field of the wire, which causes the microbeam to vibrate. Then, the mechanical vibration is converted to a voltage as the sensors' output.

2 Modeling

In this section, the two alternative configurations of the non-contact current sensors are presented. Fig. 1(a) shows the current sensor based on a parallel beam carrying current, and Fig. 1(b) shows the current sensor based on a single piezoelectric beam. For Fig. 1(a), the first configuration, the current sensor consists of two microbeams which can be made any conductive materials while Fig. 1(b), the second configuration, the current sensor has a layer of a piezoelectric material on top and bottom separated by a shim layer. Noted, the shim usually is chosen to be a metallic layer to help extracting the current produced by piezoelectric layers and reducing the equivalent stiffness of the cantilever. For simplicity of the formula, it is assumed that the wire is very long, and its cross-section is much smaller than the cross-sections of the microbeams. However, the effects of the wire's dimensions can be readily considered (Kouhpanji, 2017a, 2017b; Zamani Kouhpanji, 2018b). Thus, the magnetic field around a wire carrying current can be obtained by

$$\vec{H} = \frac{i_w}{2\pi r}\left(\cos(\alpha)\hat{e}_z - \sin(\alpha)\hat{e}_y\right) \tag{1}$$

where, i_w is the current inside the wire, which is unknown, and it can be either DC or AC; e_z is the unity vector along z-axis; e_y is the unity vector along y-axis; r is the distance of each point in the space from the wire's center, see Fig. 2. For convenience, each configuration is analyzed separately in designated sections as follows. Furthermore, all microbeams are along x-axis, and y-z plan is perpendicular to the microbeams axis.

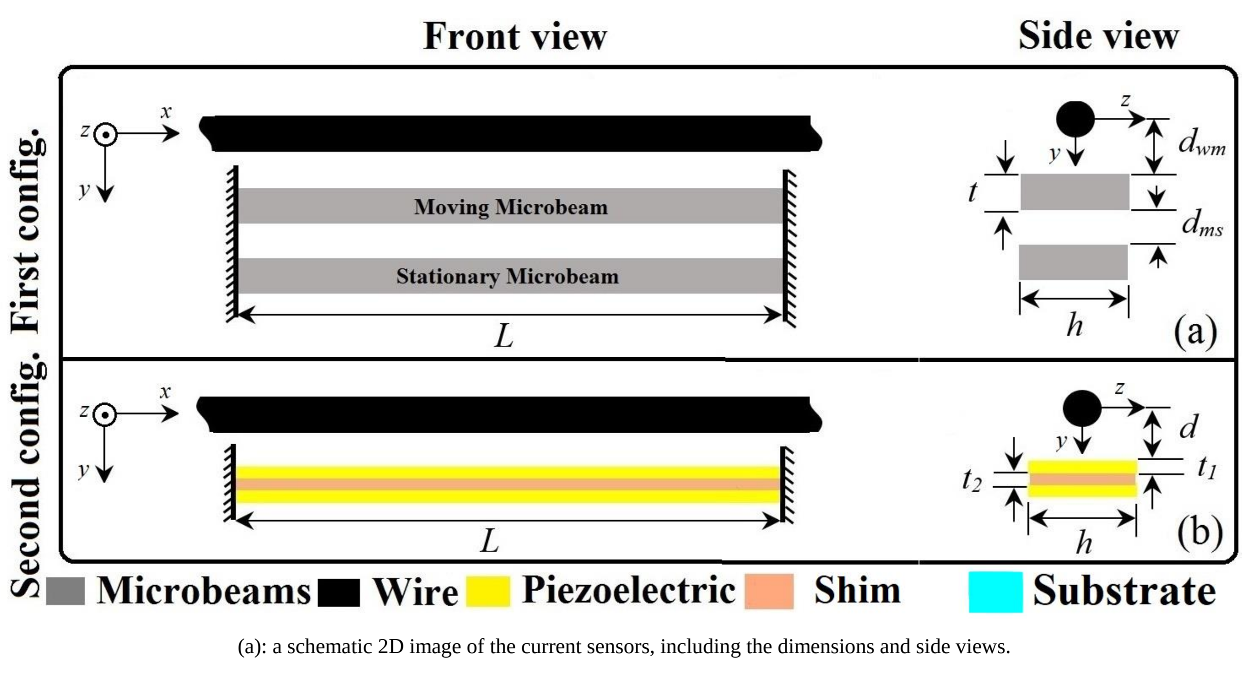

(a): a schematic 2D image of the current sensors, including the dimensions and side views.

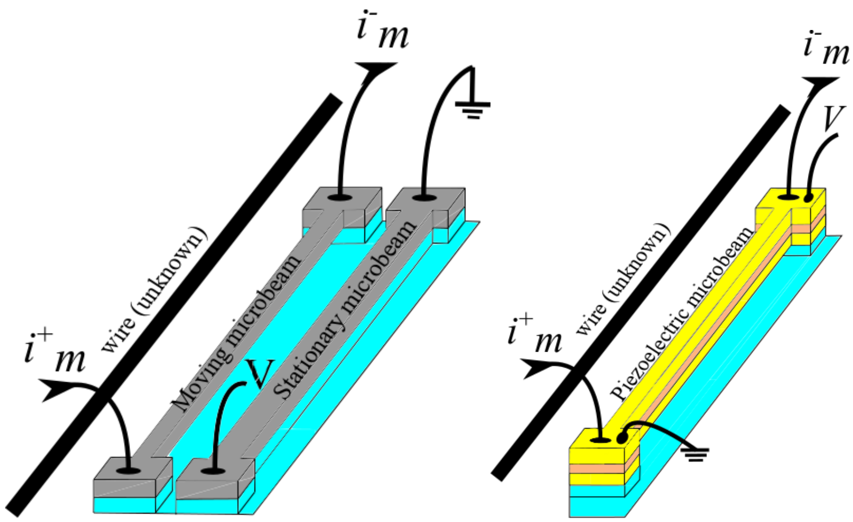

(b): a schematic 3D image of the current sensors. The left image shows the 1st configuration and the right image shows the 2nd configuration.

Fig. 1. The front view and side view of the proposed configurations for the current sensors. In the first configuration, the microbeams have the same cross-section area. For the second configuration, the two piezoelectric layers have the same cross-section dimensions, and the total cross-section area is equal to the area of the first configuration's microbeams.

2.1 The first configuration

Using Eq. (1) and the parameters presented in Fig. 1, the total force applied on the moving microbeam can be determined using Ampere Force Law (AFL) as follows

$$\vec{F} = \mu_0 L \int_{-h/2}^{h/2} \int_{d_{wm}}^{d_{wm}+t} \left(\vec{i}_m \times \vec{H}\right) dydz = -\mu \frac{i_w i_m}{2\pi} L \int_{-h/2}^{h/2} \int_{d_{wm}}^{d_{wm}+t} \left(\frac{y}{z^2+y^2} \hat{e}_y + \frac{z}{z^2+y^2} \hat{e}_z \right) dydz \tag{2}$$

where, μ_0 is the permeability of the vacuum; i_m is the current inside the microbeam; t is the thickness of the moving microbeam; h is the width of the moving microbeam; L is the length of the microbeams; and d_{wm} is the distance between the wire and the moving microbeam. Due to the symmetry condition, the force in z-direction is equal zero (Zamani Kouhpanji, 2018b). Therefore, the total force applied on the microbeam is in y-direction, and it equal to

$$F = \mu_0 \frac{i_w i_m}{2\pi} \left[\frac{h}{2} \ln\left(\frac{h^2 + 4\left(d_{wm}+t\right)^2}{h^2 + 4d_{wm}^2} \right) - 2d_{wm} \tan^{-1}\left(\frac{h}{2d_{wm}} \right) + 2\left(d_{wm}+t\right) \tan^{-1}\left(\frac{h}{2\left(d_{wm}+t\right)} \right) \right] L \tag{3}$$

Noted, the total force applied on the microbeams is in y-direction, and its direction and frequency are dependent on the product of the currents flowing in the wire and the microbeams, moving microbeam for the 1st configuration and the piezoelectric microbeam for the 2nd configuration.

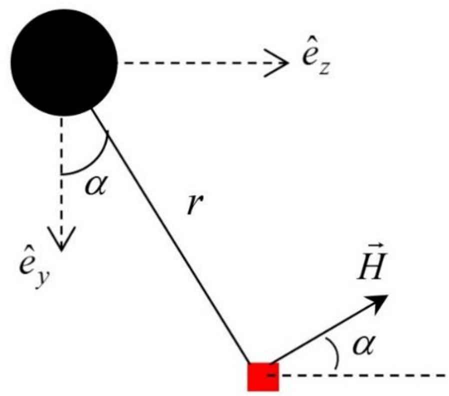

Fig. 2. Magnetic field generated around the wire due to its current.

Next step is to model the dynamic response of the moving microbeam. The moving microbeam can be modeled as a simple mass connected to a spring and damper. Therefore, the equation of motion of the moving microbeam can be written as follows

$$M\ddot{w} + \lambda\dot{w} + kw = F \tag{4}$$

where, M is the moving microbeam's mass; λ is the damping coefficient; k is the spring constant of the moving microbeam equal to $32Eht^3/L^3$, E is the Young's modulus of the moving microbeam. Furthermore, w is the displacement of the center of the moving microbeam, and the dots represent the time derivative of the displacement. Thus, the transfer function of the moving microbeam is

$$W(s) = \frac{F}{M}\frac{1}{s^2 + 2\zeta\omega_n s + \omega_n^2} \tag{5}$$

where, ζ is the damping ratio equal to $\lambda/2\sqrt{kM}$; and ω_n is the natural frequency of the moving microbeam equal to $\sqrt{k/M}$. It should be mentioned, according to (Kahrobaiyan, Asghari, Hoore, & Ahmadian, 2012), the displacement of each point along the moving microbeam can be determined by multiplying its time response (determined by solving Eq. (4)) and the eigenfunction of the moving microbeam. The eigenfunction of a continuous microbeam under fixed-fixed boundary condition, $\psi(x)$, was given (Kahrobaiyan et al., 2012)

$$\psi(x) = \cosh\left(\gamma_n \frac{x}{L}\right) - \cos\left(\gamma_n \frac{x}{L}\right) - \frac{\cosh(\gamma_n) - \cos(\gamma_n)}{\sinh(\gamma_n) - \sin(\gamma_n)}\left(\sinh\left(\gamma_n \frac{x}{L}\right) - \sin\left(\gamma_n \frac{x}{L}\right)\right) \tag{6}$$

Here, γ_n corresponds to the mode of resonant of the moving microbeam, which are the solutions of $\cosh(\gamma_n)\cos(\gamma_n)=1$.

Once the moving microbeam starts vibrating, it induces a current inside the stationary microbeam because of their relative velocity and the magnetic field generated by its current (Nayfeh & Brussel, 2015). The voltage induced between the two ends of the stationary microbeam can be determined as follows (Zamani Kouhpanji, 2018b)

$$\Delta V_m = \mu\int_0^L \left(\dot{\vec{w}} \times \vec{H}\right)dx = \frac{1}{\psi\left(\frac{L}{2}\right)A_s}\int_0^L \psi(x)dx\left(\int_{-h/2}^{h/2}\int_{d_{ms}+t}^{d_{ms}+2t} \dot{w}H_z(v_0,u_0)dv_0 du_0\right) \tag{7}$$

where, $\dot{v}$ is the velocity at the center of the moving microbeam; A_s is the cross-section area of the stationary microbeam; d_{ms} is the distance between the moving microbeam and stationary microbeam; and H_z is the magnetic field generated by the moving microbeam in z-direction determined by (Feynman, Leighton, & Sands, 2013)

$$H_x(v_0, u_0) = \frac{i_m}{2\pi A_m} \int_{-h/2}^{h/2} \int_0^t \frac{v_0 - v}{(u_0 - u)^2 + (v_0 - v)^2} dv du \tag{8}$$

where, A_m is the cross-section area of the moving microbeam; and u-v are the axes of the coordinate system located on the center of the upper face of the moving microbeam while the x-axis is along the moving microbeam's axial axis. Moreover, the (u, v) and (u_0, v_0) represent points on the moving and stationary microbeam, respectively, at this coordinate system.

It is noteworthy to be mentioned that the frequency of the output signal in this configuration is a combination of the frequencies of the wire's current and the moving microbeam's current because the output signal is a result of products of the currents which have sinusoidal terms according to their frequency. However, if the wire's current is a DC current, the output signal frequency is only dependent on the frequency of the microbeam's current, and it has the following time-dependent term

$$\frac{d}{dt}(\sin(\omega_m t))\sin(\omega_m t) = \frac{\omega_m}{2}\sin(2\omega_m t) \tag{9}$$

If the wire has an AC current, then the output signal has the following time-dependent term (left side of Eq. (10) which can simplified to summation as the right side of following equation

$$\frac{d}{dt}(\sin(\omega_w t)\sin(\omega_m t))\sin(\omega_m t) = \frac{\omega_w}{2}\cos(\omega_w t) - \frac{\omega_w + \omega_m}{4}\cos((\omega_w + 2\omega_m)t) - \frac{\omega_w - \omega_m}{4}\cos((\omega_w - 2\omega_m)t) \tag{10}$$

where, t is time; ω_w is the frequency of the wire's current; and ω_m is the frequency of the moving microbeam's current.

2.2 The second configuration

The force applied on each layer of the piezoelectric microbeam can be calculated using Eq. (3), and the total force applied on the piezoelectric microbeam is the summation of all forces. Noted that the total current flowing in the piezoelectric microbeam is the summation of all current flowing in each layer. To determine each layer current, the piezoelectric microbeam can be modeled as three parallel resistances. Furthermore, it should be mentioned that the force applied on the piezoelectric microbeam is mainly due to the input current, not the current induced inside it by mechanical vibration. That is why the induced current is usually several orders of magnitude smaller than the input current.

Modeling the dynamical vibration of the piezoelectric microbeam is completely different from a regular microbeam, such as the 1st configuration. First, the piezoelectric microbeam is made of three layers where each layer can have different mechanical properties and thicknesses. Therefore, the equivalent stiffness, $(EI)_{eq}$, of the microbeam must be considered to take into account the variations of the materials properties and sized on the mechanical stiffness. The equivalent mechanical stiffness can be determined using

$$(EI)_{eq} = \sum_{j=1}^{3} E_j I_j = 2E_{PZ}\left(\frac{1}{12}ht_1^3 + t_1 h\left(\frac{t_1}{2}+\frac{t_2}{2}\right)^2\right) + \frac{1}{12}E_d h t_2^3 \tag{11}$$

where, t_1 is the thickness of the piezoelectric layers; h is the width of the piezoelectric layers which it is equal to the shim layer width; t_2 is the thickness of the shim layer; E_{PZ} is the Young's modulus of the piezoelectric layers; and E_d is the Young's modulus of the shim layer.

Second, because of the existence of the charges on the piezoelectric layers impact the mechanical behavior of the piezoelectric, the governing equations of motion for piezoelectric microbeam are electromechanically coupled. The governing equations of motion for piezoelectric microbeams under forced vibration was derived by (Roundy & Wright, 2004) using analogy within the electrical circuit and mechanical structures. (Roundy & Wright, 2004) derived the equation of motion of a piezoelectric microbeam as

$$\begin{aligned} &\ddot{S} + 2\zeta\omega_n \dot{S} + \omega_n^2 S = \frac{k_{sp} a_1 d_{31}}{M_{eq}} V + \frac{F}{k_2 M_{eq}} \\ &\dot{V} = \frac{a_3 c_p d_{31} t_1}{a_2 \varepsilon} \dot{S} \end{aligned} \tag{12}$$

where, S is the axial strain inside the piezoelectric layers and the dots again show the time derivative of the axial strain; V is the voltage between the two ends of the piezoelectric microbeam; M_{eq} is the equivalent mass of the piezoelectric microbeam which is equal to the summation of all layers masses; d_{31} is the piezoelectric coefficient of the piezoelectric layers; c_p is the capacitance induced between the piezoelectric layers due to accumulation of charges; the a_1, a_2 and a_3 are the coefficients related to the configurations between the piezoelectric layers; k_{sp} is the spring constant of the piezoelectric microbeam equal to $384(EI)_{eq}/L^3$. Lastly, k_2 is a geometric coefficient depending on the boundary condition, dimension and the length of the piezoelectric microbeam at boundaries, L_e. The k_2 for a fixed-fixed boundary condition is equal to

$$k_2 = \frac{L^4}{32t_1}\frac{1}{2L^2 - 3LL_e + L_e^2} \tag{13}$$

By solving the Eq. (12), the AC voltage induced between the two ends of the piezoelectric microbeam can be achieved as (Leland et al., 2008)

$$\Delta V_{pz} = \frac{1}{s^2 + 2\zeta\omega_n s + \omega_n^2\left(1 - \frac{d_{31}c_p}{\varepsilon}\right)} \frac{d_{31}c_p t_1 a_3}{k_2 M_{eq}\varepsilon a_2} F \tag{14}$$

where, ε is the dielectric constant of the piezoelectric layers.

The force applied on the microbeam in the 2nd configuration is due to interaction between the magnetic field induced by the current of the wire and microbeam. According to Equ. (3), this force has the product of the both currents. If the wire carries an AC current, its output signal will have the product of the sinusoidal functions as $\sin(\omega_w t)\sin(\omega_{pz} t)$, which can be readily simplified as follows

$$\sin(\omega_w t)\sin(\omega_{pz} t) = \frac{1}{2}\cos((\omega_w - \omega_{pz})t) - \frac{1}{2}\cos((\omega_w + \omega_{pz})t) \tag{15}$$

where, ω_{pz} is the frequency of the piezoelectric microbeam's current. And, if the wire has a DC current, then the frequency of the output signal will be equal to the frequency of the piezoelectric microbeam's current. If the frequency of the wire is known, the frequency of the microbeam must be selected such as $\omega_m=\omega_w-\omega_n$ or $\omega_m=\omega_n-\omega_w$, where ω_n is the resonance frequency of the microbeam. In this case, the force applied on the microbeam will have at least one component at the resonance frequency of the microbeam leading in the largest mechanical vibration amplitude for the microbeam, consequently, highest signal-to-noise ratio at the output. In practical application, if the frequency of the wire is unknown, the user must conduct a sweep mode frequency measurement to see the response of the current sensor, as it must be done for all current sensors. Once a sweep mode frequency measurement is conducted, there will be an output response associated with each of these frequencies. Then, by using the provided formulas, one can easily determine the frequency of the wire, even if it is unknown, as well as the required frequency for the microbeam for further detections. The similar argument is valid for the 1st current sensor configuration.

3 Results and discussions

The materials properties were taken from (Xiang & Shi, 2009), for the piezoelectric layers, and (Rumble, 2017) for the silicon microbeams and aluminum shim. Table. 1 provides the physical parameters used for modeling and evaluating the designs.

Table. 1: used parameters for modeling of the current sensors.

Parameters	1st Configuration	2nd Configuration
Thickness of the moving and stationary beam (t)	1E-6 m	-
Thickness of top piezoelectric later (t_1)	-	0.33E-6 m
Thickness of the bottom piezoelectric layer (t_2)	-	0.33E-6 m
Width of the microbeams (h)	1E-6 m	
Length of the microbeams (L)	1E-3 m	
Distance between the moving microbeam and the wire (d_{wm})	2E-6 m	
Distance between the stationary microbeam and the wire (d_{ms})	2E-6 m	-

Figs. 3 and 4 demonstrate the dynamic response of the current sensors by presenting the gain and phase shift of the current sensors. As it can be seen, the maximum gains decrease as the damping ratio increases. In the proposed current sensors, the damping is due to the structural damping and viscous damping induced by the interaction between the microbeams and the air surrounding the current sensors, where the structural damping has the dominant impact on the performance of the current sensors. The structural damping can be significantly reduced by either increasing the length of the microbeams or decreasing the cross-section dimensions of the microbeams. Noted the phase shift of the two configurations are completely different from each other even though their gains are almost the same. For the 1st configuration, the phase shift is equal to zero at the resonance frequency, and it varies smoothly at the vicinity of the resonance frequency. However, for the 2nd configuration, the phase shift has a discontinuity at the resonance frequency, and it has 180 degrees phase shift.

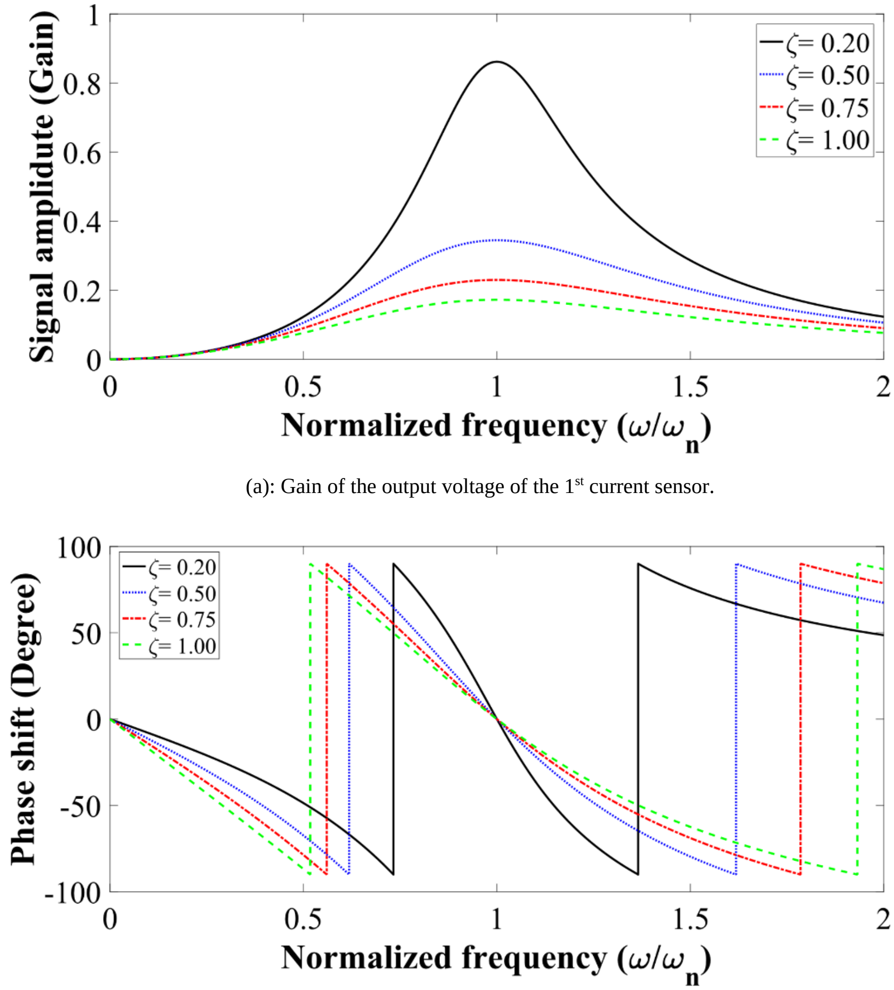

(a): Gain of the output voltage of the 1st current sensor.

(b): Phase shift of the output voltage of the 1st current sensor.

Fig. 3. Dynamical response of the 1st current sensor. (a) Gain, (b) phase shift.

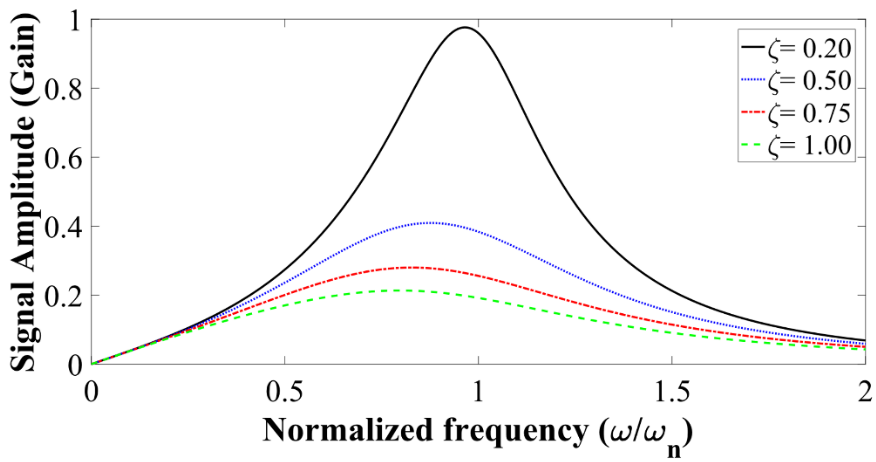

(a): Gain of the output voltage of the 2nd current sensor.

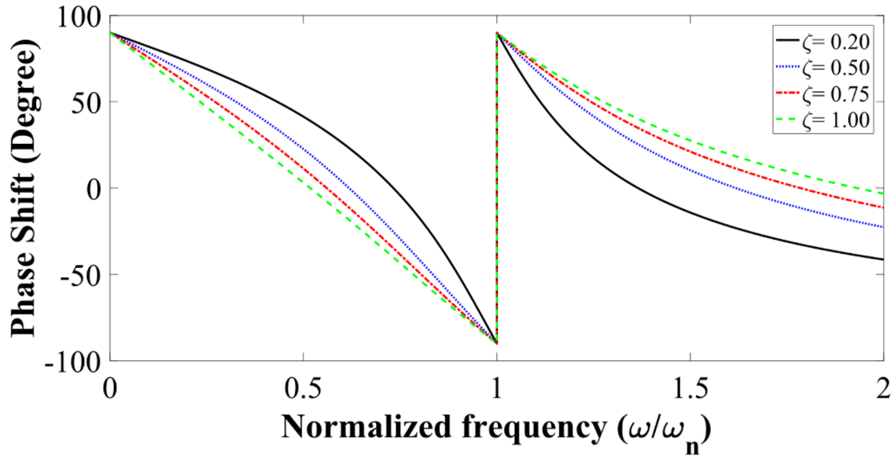

(b): Phase shift of the output voltage of the 2nd current sensor.

Fig. 4. Dynamical response of the 2nd current sensor. (a) Gain, (b) phase shift.

It should be mentioned that the position of the maximum gain of the 1st current sensor is only dependent on the moving microbeam natural frequency and the damping ratio, while it depends on the piezoelectric coefficient, dielectric constant, and piezoelectric capacitance in addition to the natural frequency and damping ratio of the 2nd current sensor, see Eq. (14). This fact causes the position of the maximum gain of the 2nd current sensor to be more dependent on the damping ratio which can be seen as a small shift on the position of the maximum gain of the 2nd current sensor comparing to the 1st current sensor, see Fig. 5.

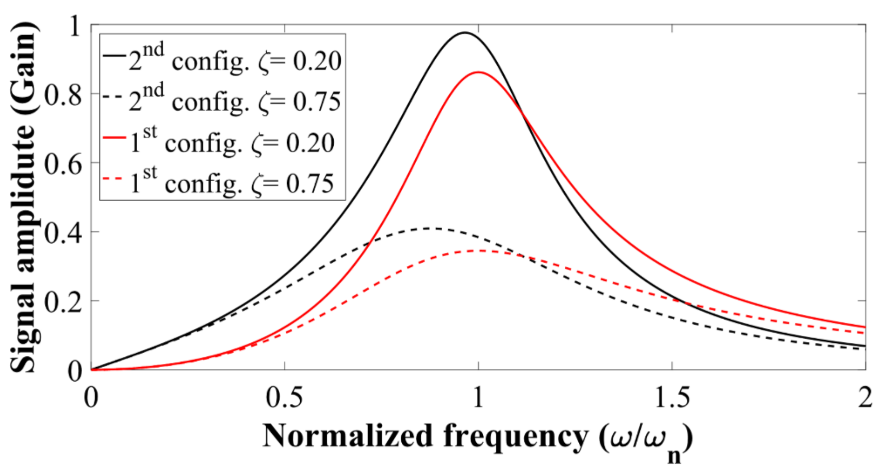

Fig. 5. Comparing the gain of the current sensors.

One of the critical factors in designing any sensor is the real-time sensitivity of the sensor. The real-time sensitivity is defined as derivative of the output signal to the input signal of the sensor. According to Eqs. (7) and (14), the output signal in both current sensors are linearly proportional to the input currents, which is one of the superior advantages of these configurations comparing to the prior current sensors. This linear behavior of the current sensors results the real-time sensitivity of the current sensors to be the same as their time responses without any dependency on the wire frequency, wire current amplitude or physical parameters of the wire. This superior advantage of these current sensors makes it possible to optimize an initial design of these current sensors, then it can be used for any input signal with the same performance. Therefore, the real-time sensitivity of the proposed current sensors is

$$\text{Sensitivity} \equiv \frac{d(\Delta V)}{dI} \tag{16}$$

where, ΔV is the output voltage of the current sensors; and I is the product of the amplitudes of the unknown current inside the wire and the current of the microbeams. Fig. 6 depicts the time response of the current sensors for a sinusoidal input signal. In Fig. 6, all physical parameters are assumed to be the same for both current sensors, where the total thickness of the piezoelectric microbeam is the same as the moving and/or stationary microbeams' thickness. The initial parts of the time response, equivalently, the real-time sensitivities, of the current sensors are affected by the transient response of the sensors, and they reach the steady state conditions after a few cycles. It should be emphasized that the 1st configuration provides a faster dynamic response comparing to the 2nd configuration for the same conditions.

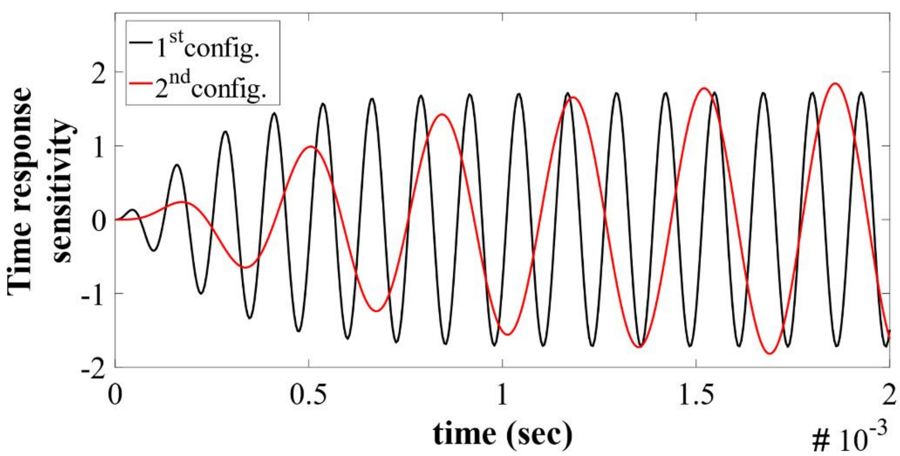

Fig. 6. Time response of the current sensors for a sinusoidal input current with ζ= 0.5, the frequency of the wire and microbeam is assumed to be equal to the half of the resonance frequency of the microbeam.

The power consumption of the current sensors is also analyzed which is another critical factor in designing high efficient current sensors. In both configurations, the input power is related to the power consumed in the microbeams for generating the mechanical vibration. Therefore,

$$\begin{aligned} &1^{st}\text{ configuration:} && P_{in} = i_m^2 R_m \\ &2^{nd}\text{ configuration:} && P_{in} = i_{pz}^2 R_{pz} \end{aligned} \tag{17}$$

where, i_{pz} it the input current in the piezoelectric microbeam; R_m is the electrical resistance of the moving microbeam; and the R_{pz} is the electrical resistance of the piezoelectric microbeam. Another superior advantage of these configurations comparing to previous current sensors is that the consumed power is only dependent on the electrical resistance of the microbeams and the input current. On the other hand, according to Eqs. (7) and (14), since the output signal is independent on the electrical resistance of the microbeams, the power consumption can be minimized to zero by increasing the doping level into the microbeams or using a metallic moving microbeam for the 1st configuration.

To investigate the power efficiency, P_{out}/P_{in}, of the current sensors, here the output power of the current sensors is calculated. Since the output signal is a voltage, thus the output power is

$$
\begin{aligned}
&\text{1st configuration:} \qquad P_{out} = \frac{\Delta V_m^2}{R_s} \\
&\text{2nd configuration:} \qquad P_{out} = \frac{\Delta V_{pz}^2}{R_{pz}}
\end{aligned}
\tag{18}
$$

where, R_s is the electrical resistance of the stationary microbeam which is the same as R_m. Fig. 7 shows the normalized power efficiency of the current sensors.

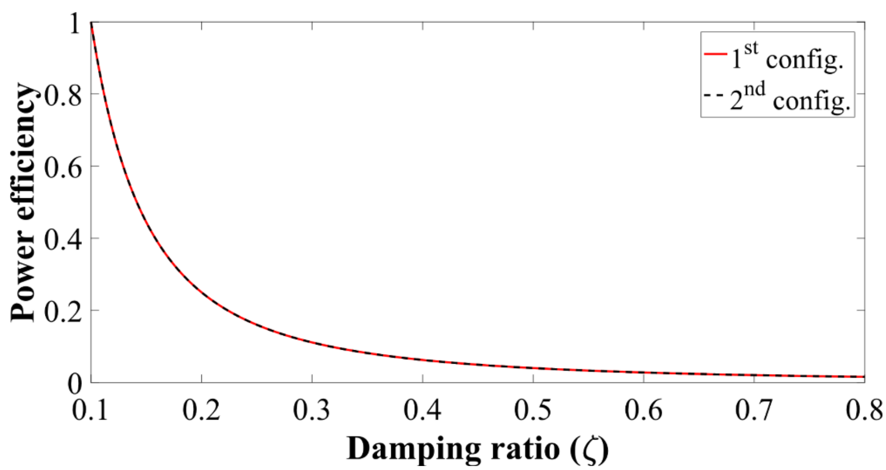

Fig. 7. Power efficiency of the current sensors normalized to the power efficiency at $\zeta = 0.10$. For simplicity, it is assumed that the wire carries a DC current, and the microbeams carry a current at their resonance frequency.

As it can be seen from Fig. 7, the power efficiency of the current sensors is the same for the same physical parameters, and it only depends on the damping ratio of the sensors. Noted, even though the power efficiency of the current sensors is the same, their output power could be different due to different electrical resistance of the microbeams, see Eqs. (18). Table 2 is provided to summarize the state-of-art of the proposed current in a nutshell. For the sake of comparison, it is assumed that the both configurations have the same dimensions.

Table 2: Qualitative comparison between the two configurations.

Practical concern	1st configuration	2nd configuration
Sensitivity	Good	Medium
Power consumption	Good	Good
Signal to noise ratio	Medium	Good
Linearity in response	Good	Medium
Fabrication process	Medium	Complicated

4 Conclusion

Here two different non-invasive current sensors are proposed, designed and analyzed based on the Ampere Force Law (AFL). The current sensors are able to detect/sense both DC, AC or their combinations in a single wire or multi-wire network. For the same physical parameters, the 1st configuration (current sensor using two parallel microbeams) presents a faster dynamic response comparing to the 2nd configuration (current sensor using a piezoelectric microbeam). However, the 2nd configuration presents a higher gain comparing to the 1st configuration. Furthermore, experimentally wise, the 2nd configuration is more difficult to be fabricated due to the required extra steps for implementing the piezoelectric material on the microbeam. The dynamic response and the sensitivities of the current sensors are linearly dependent on the wire current and wire frequency. The power consumption of the current sensors is examined, and it was found that the power consumption of the current sensors is only dependent on the electrical resistance of the microbeams, which demonstrates extremely low power consumption for the current sensors. Furthermore, studying the power efficiency of the current sensors showed that there is not any tradeoff or dependency between the power consumption and the sensitivity and the dynamic response of the current sensors. Therefore, it can be concluded that the sensitivity and dynamic response of the current sensors can be maximized without affecting the power efficiency of these current sensors. Furthermore, the dynamic response analysis, sensitivity analysis, and power consumption analysis of the proposed current sensors confirm the practical realization of the proposed current sensors in both industrial and household applications.

References

Breth, L., Dimopoulos, T., Schotter, J., Rott, K., Bruckl, H., & Suess, D. (2011). Fluxgate principle applied to a magnetic tunnel junction for weak magnetic field sensing. *IEEE Transactions on Magnetics*, *47*(6 PART 1), 1549–1553. https://doi.org/10.1109/TMAG.2011.2106114

Cao, X., jian Tian, X., & Wang, D. F. (2017). Wireless electric current sensing via integrating a magnetic-piezoelectric cantilever with a micro-strip antenna. *Micro & Nano Letters*.

Chattock, A. P. (1887). *On a Magnetic Potentiometer*. *Proceedings of the Physical Society of London* (Vol. 9). https://doi.org/10.1088/1478-7814/9/1/305

Feynman, R. P., Leighton, R. B., & Sands, M. (2013). *The Feynman Lectures on Physics, Desktop Edition Volume I* (Vol. 1). Basic books.

Hui, Y., Nan, T. X., Sun, N. X., & Rinaldi, M. (2013). MEMS resonant magnetic field sensor based on an AlN/FeGaB bilayer nano-plate resonator. *2013 IEEE 26th International Conference on Micro Electro Mechanical Systems (MEMS)*, (1), 721–724. https://doi.org/10.1109/MEMSYS.2013.6474344

Jackson, N., Olszewski, O. Z., O'Murchu, C., & Mathewson, A. (2017). Shock-induced aluminum nitride based MEMS energy harvester to power a leadless pacemaker. *Sensors and Actuators A: Physical*, *264*, 212–218. https://doi.org/10.1016/j.sna.2017.08.005

Julliere, M. (1975). Tunneling between ferromagnetic films. *Physics Letters A*, *54*(3), 225–226. https://doi.org/10.1016/0375-9601(75)90174-7

Kahrobaiyan, M. H., Asghari, M., Hoore, M., & Ahmadian, M. T. (2012). Nonlinear size-dependent forced vibrational behavior of microbeams based on a non-classical continuum theory. *Journal of Vibration and Control*, *18*(5), 696–711. https://doi.org/10.1177/1077546311414600

Kouhpanji, M. R. Z. (2017a, November). Designing and Analyzing Sensor and Actuator of a Nano/Micro-System for Fatigue and Fracture Characterization of Nanomaterials . *International Journal of Mechanical, Aerospace, Industrial, Mechatronic and Manufacturing Engineering*.

Kouhpanji, M. R. Z. (2017b, December). Studying the Dynamical Response of Nano-Microelectromechanical Devices for Nanomechanical Testing of Nanostructures . *International Journal of Mechanical, Aerospace, Industrial, Mechatronic and Manufacturing Engineering*.

Kouhpanji, M. R. Z., Behzadirad, M., Feezell, D., & Busani, T. (2018). Insufficiency of the Young's modulus for illustrating the mechanical behavior of GaN nanowires. *Nanotechnology*, *29*(20), 205706.

Leland, E. S., White, R. M., & Wright, P. K. (2006). Energy scavenging power sources for household electrical monitoring. *PowerMEMS (Dec. 2006)*, 165–168.

Leland, E. S., White, R. M., & Wright, P. K. (2008). Design and Fabrication of a MEMS AC Electric Current Sensor. *Advances in Science and Technology*, *54*, 350–355. https://doi.org/10.4028/www.scientific.net/AST.54.350

Lin, Q. Bin, & Du, G. T. (2011). The study of a MEMS magnetic field sensor based on �cross-shape� ferromagnetic film. In *Materials Science Forum* (Vol. 694, pp. 523–527).

Nayfeh, M. H., & Brussel, M. K. (2015). *Electricity and magnetism*. Courier Dover Publications.

Olszewski, O. Z., Houlihan, R., Blake, A., Mathewson, A., & Jackson, N. (2017). Evaluation of Vibrational PiezoMEMS Harvester That Scavenges Energy From a Magnetic Field Surrounding an AC Current-Carrying Wire. *Journal of Microelectromechanical Systems*.

Ramsden, E. (2011). *Hall-effect sensors: theory and application*. Newnes.

Reza, M., & Kouhpanji, Z. (2017). UNM Digital Repository Investigating the classical and non-classical mechanical properties of GaN nanowires. *MS. Thesis, University of New Mexico*, 1–83.

Roundy, S., & Wright, P. K. (2004). A piezoelectric vibration based generator for wireless electronics. *Smart Materials and Structures*, *13*(5), 1131–1142. https://doi.org/10.1088/0964-1726/13/5/018

Rumble, J. (2017). *CRC handbook of chemistry and physics*. CRC press.

Sensitivity, T. (2014). Design, Fabrication and Temperature Sensitivity Testing of a Miniature Piezoelectric-Based Sensor for Current Measurements, 162–181. https://doi.org/10.3390/act3030162

Shang, X., Li, Y., Liu, H., Kobayashi, T., Wang, D. F., Itoh, T., & Maeda, R. (2017). Developing MEMS DC electric current sensor for end-use monitoring of DC power supply: Part VI�Corresponding relationship between sensitivity and magnetic induction. In *Design, Test, Integration and Packaging of MEMS/MOEMS (DTIP), 2017 Symposium on* (pp. 1–4).

Sherman, C. T., Wright, P. K., & White, R. M. (2016). Sensors and Actuators A : Physical Validation and testing of a MEMS piezoelectric permanent magnet current sensor with vibration canceling. *Sensors & Actuators: A. Physical*, *248*, 206–213. https://doi.org/10.1016/j.sna.2016.06.022

Wang, D. F., Liu, H., Li, X., Li, Y., Xian, W., Kobayashi, T., … Maeda, R. (2017). Passive MEMS DC Electric Current Sensor : Part I — Theoretical Considerations, *17*(5), 1230–1237.

Wang, D. F., & Maeda, R. (2015). Analytical study on cantilever resonance type magnet-integrated sensor device for micro-magnetic field detection. *Microsystem Technologies*, *21*(6), 1167–1172. https://doi.org/10.1007/s00542-014-2167-y

Ward, D. a., & Exon, J. L. T. (1993). Using Rogowski coils for transient current measurements. *Engineering Science and Education Journal*, *2*(3), 105. https://doi.org/10.1049/esej:19930034

Xian, W., Li, X., Wang, D. F., Kobayashi, T., Itoh, T., & Maeda, R. (2017). Precise current sensing using a piezoelectric cantilever based current sensor. In *2017 19th International Conference on Solid-State Sensors, Actuators and Microsystems (TRANSDUCERS)* (pp. 1057–1060). https://doi.org/10.1109/TRANSDUCERS.2017.7994234

Xian, W., & Wang, D. F. (2017). Position and orientation correction scheme for current sensing based on magnetic piezoelectric cantilevers, *143501*, 1–12. https://doi.org/10.1063/1.4979787

Xiang, H. J., & Shi, Z. F. (2009). Static analysis for functionally graded piezoelectric actuators or sensors under a combined electro-thermal load. *European Journal of Mechanics, A/Solids*, *28*(2), 338–346. https://doi.org/10.1016/j.euromechsol.2008.06.007

Zamani Kouhpanji, M. R. (2018a). Demonstrating the effects of elastic support on power generation and storage capability of piezoelectric energy harvesting devices. *Journal of Intelligent Material Systems and Structures*, 1045389X1880639. https://doi.org/10.1177/1045389X18806398

Zamani Kouhpanji, M. R. (2018b). Paired-wire carrying current actuators and piezoelectric beam sensors for microelectromechanical systems. *Microsystem Technologies*, *24*(5), 2401–2408. https://doi.org/10.1007/s00542-018-3722-8

Zamani Kouhpanji, M. R., Behzadirad, M., & Busani, T. (2017). Classical continuum theory limits to determine the size-dependency of mechanical properties of GaN NWs Classical continuum theory limits to determine the size-dependency of mechanical properties of GaN NWs. *Journal of Applied Physics*, *225113*(22), 225113. https://doi.org/10.1063/1.5000016

Zamani Kouhpanji, M. R., & Jafaraghaei, U. (2017). A semianalytical approach for determining the nonclassical mechanical properties of materials. *Journal of the Mechanical Behavior of Materials*. https://doi.org/10.1515/jmbm-2017-0025

Ziegler, S., Woodward, R. C., Iu, H. H.-C., & Borle, L. J. (2009). Current Sensing Techniques: A Review. *IEEE Sensors Journal*, *9*(4), 354–376. https://doi.org/10.1109/JSEN.2009.2013914